32nd URSI GASS, Montreal, 19–26 August 2017

Prelaunch Performance of the 118.75 GHz PolarCube 3U Temperature Sounding Radiometer

Lavanya Periasamy and Albin J. Gasiewski
Department of Electrical, Computer, and Energy Engineering,
University of Colorado, Boulder, CO.

Abstract

Design, analysis and pre-launch performance of the PolarCube 3U CubeSat 118.75 GHz radiometer payload is presented. Procedures used to determine optimum feed horn/reflector dimensions, phase center and antenna efficiencies based on a full wave Fourier analysis are outlined. A brief description of the design and functionality of the eight channel intermediate frequency board is also provided. Images obtained by the instrument during recent airborne tests over the Antarctic using an aluminium 3D printed corrugated feed indicate a well focused scanning reflector antenna system with high main beam efficiency and good separation between the radiometer channels.

1 Introduction

The development of a fleet of passive microwave sensors especially at V-band and higher frequencies in low earth orbit using 3U and 6U CubeSats could help accomplish acquisition of meteorological data at high spatial and temporal resolution at low system cost and risk as well as provide for regularly updated sensor technology. The University of Colorado's 3U CubeSat, PolarCube is intended to serve as a demonstrator for such a fleet of passive sounders and imagers. PolarCube is a 3U CubeSat with ∼1.5U (i.e) 15 cc available for the radiometer payload. The mission is focused primarily on sounding in Arctic and Antarctic regions with the following key remote sensing science and engineering objectives: (i) atmospheric profiling by passive sounding using the 118.7503 GHz O_2 resonance with a focus on observing tropospheric temperature structure [1] above partially open-water areas at high latitudes (ii) resolving sea ice edges and mapping sea ice concentration and associated temperature variations under both clear and cloudy atmospheric conditions (iii) assess the capabilities of small passive microwave satellite sensors for environmental monitoring in support of the future development of inexpensive earth science missions.

2 Instrument Description

PolarCube is a 3U CubeSat satellite based on an existing bus design supporting an eight channel, double sideband 118.75 GHz scanning passive microwave temperature sounder, MiniRad (Figure 1). A 3D printed corrugated feedhorn illuminates an 8 cm offset scanning parabolic reflector to achieve a 2.3° beam width with nominal one second scan period. The radiometer implements a two-point calibration using an internal PIN switch and view of cold space. The RF front end of the total power radiometer includes a sub-harmonic mixer/tripler, dielectric resonator oscillator and low noise amplifier. The IF module comprises of an 8 channel filterbank selected to sample vertically from the surface to ∼18 km altitude. The estimated radiometer sensitivity, ΔT_{rms} for 3 dB sampling and integration time of 4 ms varies from 0.3 K to 2 K across the eight channels. The performance of the dielectric resonant oscillator, low noise amplifier and IF surface mount amplifiers have been characterized at different operating voltages so that these components can be operated in a power starved mode for optimum performance.

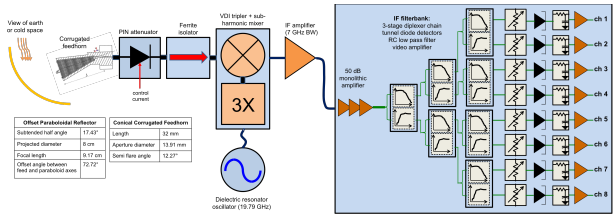

Figure 1. Functional block diagram of the radiometer payload

3 PolarCube Antenna Sub-system

Radiometric sounding measurements used to provide climate and weather data are strongly affected by the main-beam, ohmic, and spillover efficiencies of the optics, as well as inhomogeneities in the scene and background radiation fields. Errors in estimating the antenna system's phase center as well as surface errors in the focussing element also produce a phase non-uniformity in the main aperture fields. The interpretation of radiometric data is also affected by the accuracy with which these efficiencies can be determined. To emphasize this point, it is to be noted that a space-borne radiometer observing a 300 K scene in cold space requires that the error in the estimation of spillover efficiency be 0.03% or smaller in order to obtain corrected brightness temperature measurement accuracies of 0.1 K

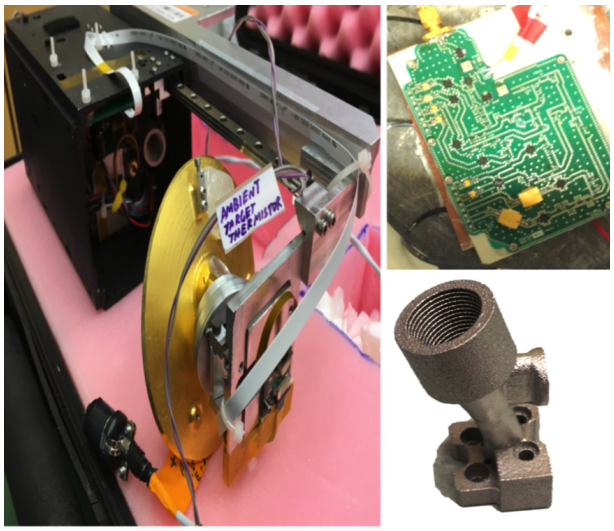

Figure 2. Left to right: (a) MiniRad instrument packaged for Operation IceBridge (b) populated IF board (c) 3D printed corrugated feed horn with bent waveguide transition

or better. To provide a more precise determination of the requisite efficiencies for radiometry, a rigorous numerical analysis of the complex diffracted field produced by a corrugated feed [2] located at the focal point of a spinning offset paraboloidal reflector was implemented using a full wave Fourier field method [3]. The analysis lead to determination of an optimal feed horn and reflector geometry such that the main beam and spillover efficiencies of the antenna system are maximized, and these and the phase center of the antenna are precisely known (Figure 5a). This information is needed for spinning reflector/fixed-feed systems at all scan angles. It enables precise knowledge of the antenna's spatial radiometric response before launch and is especially critical for radiometers that do not permit end-to-end calibration such as the PolarCube 118.7503 GHz radiometer.

The antenna subsystem of the PolarCube radiometer payload comprises of a spinning offset paraboloidal main reflector and a stationary conical corrugated feed (Figure 2). The reflector is supported by a single strut that minimizes sidelobe scattering and antenna temperature uncertainty. Taking into the account the desired gain of the feed, spillover and aperture illumination efficiencies at the reflector and, the space constraints within the 3U CubeSat, a corrugated feed horn of length $\sim$32 mm and diameter 5.5λ was designed. The PolarCube reflector's dimension of 8 cm across its minor axis was chosen to provide a $\sim$18 km footprint from an orbit altitude of $\sim$400 km. A slightly larger major axis dimension of $\sim$10 cm was chosen based on the the volume available for stowing the mirror inside the CubeSat volume. Due to this offset geometry and the fixed position of the RF front end inside the CubeSat, the feed horn has a 17.3° bent rectangular to circular waveguide transition. After optimizing the geometry of the waveguide and corrugations in HFSS, this aluminium feed designed to operate between 110 GHz and 127 GHz was manufactured by a 3D printing process for a fraction of the cost of an electroformed horn. The far field beam efficiency of the 3D printed horn obtained using measurements made at the CROMMA facility [4] show that if the MiniRad reflector were in the far field of the feed horn, $\sim$90.8% of the feed's total energy will be contained within its aperture. This is close to the theoretical estimate of $\sim$92% (Figure 3).

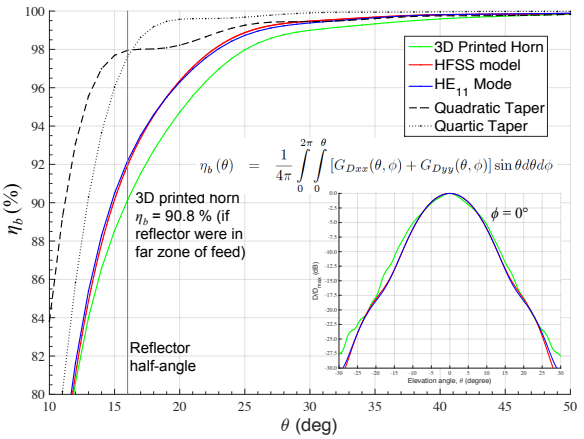

Figure 3. Measured and computed far field main beam efficiency curves of the 3D printed feed horn are shown. η_b for the 3D printed horn is $\sim$1% lower than that computed using the HE_{11} mode aperture field distribution and the HFSS model. The inset is a plot of the measured and computed normalized far field directivity patterns for the $\phi = 0°$ plane.

Held by a single strut in its deployed configuration, the reflector's focal length of 9.18 cm was chosen based on the fixed length of the instrument's RF chain, theoretical estimate of the feed horn phase center (5a) and a reasonable $F\#$. The mechanical assembly enables a few degrees of freedom of movement of the mirror so that its focus can coincide with the horn's virtual phase center. After the focusing, the PolarCube spillover efficiency at the reflector (for scan angle $\phi_s = 0°$) was computed to be $\eta_s = 95.47\%$ at its center frequency. The main aperture illumination pattern is slightly asymmetric due to the offset geometry. This asymmetry in the main aperture illumination consequently produces a small but unavoidable asymmetry in the main antenna beam. It is also important to know contributions from the sidelobes (Figure 4) due to the spillover fields from the feed horn. The total far fields can be used to compute the expected main beam efficiency of the antenna system for PolarCube. A main beam efficiency of $\sim$87% is expected (Figure 5b). Far field pattern measurements for the antenna system will be completed shortly.

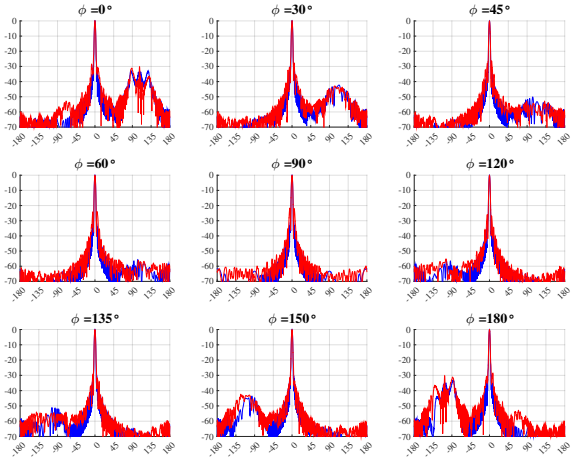

Figure 4. Comparisons between the full wave (in blue) and HFSS (in red) total far field patterns for several azimuthal cuts indicate that sidelobes due to spillover fields from the feedhorn are most prominent closer to $\phi = 0^\circ$.

4 Filterbank Design and Performance

To meet the tight volume constraints inside the CubeSat, a low cost, light weight and compact intermediate frequency (IF) module was developed that fit on a 9 cm x 5 cm two-layer RO4350B printed circuit board (Figure 2b). It includes two stage surface mount amplifiers, an eight channel filter bank and detector circuitry. The filter bank is designed as parallel connected, partly complementary structures with Chebyshev low and band/ high pass filters. The circuit was designed taking into account effects of parasitics in the cascaded diplexer model due to the coplanar waveguide and lumped element combination model. The measured response of the filterbank (Figure 6a) includes measured responses of the IF low noise amplifier and 2-stage monolithic surface mount amplifiers. The taper in the $|S_{21}|$ with increasing frequency is due to the roll-off in gain of the surface mount amplifiers. The convolutional bandwidths for the channels vary from 200 MHz to 3000 MHz and and the corresponding receiver sensitivities have been computed to be between 1.8 K and 0.3 K. A second board comprising eight video amplifiers for each IF channel and ADC circuitry is connected under the IF board with a thin layer of Eccosorb® sandwiched in between to prevent any unwanted coupling. Thermal tests ($-18^\circ C$ to $+50^\circ C$) to determine the sensitivity of the IF board to temperature variations indicated responses that were stable and gain variations within acceptable limits that could be corrected with thermopads. A comparison between the atmospheric temperature weighting functions over polar ocean for nadir observation (Figure 6b) obtained using a microwave radiative transfer program using both measured and simulated filterbank responses indicates close agreement between the two cases.

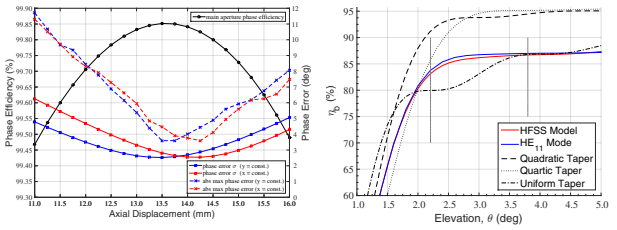

(a) (b)

Figure 5. (a) Computed phase efficiency and phase error standard deviation curves (at 118.7503 GHz) on the main aperture plane for axial displacements of the reflector along the feed axis are depicted. Displacements are measured into the feed with respect to it's aperture. The PolarCube reflector was aligned using the estimated virtual phase center (13.5 mm) where the main aperture phase efficiency is maximized. (b) Total far field main beam efficiencies computed using full wave and HFSS models are shown. Gray lines mark first nulls for a uniform illuminated aperture and the PolarCube antenna.

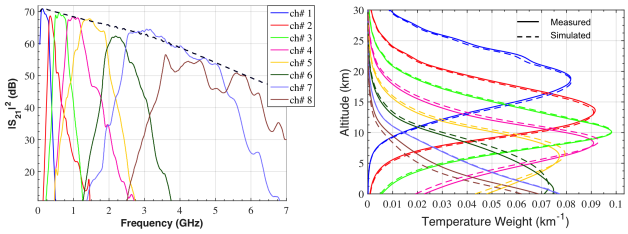

(a) (b)

Figure 6. Measured filterbank responses (with system gain) and computed weighting functions (winter, ocean, nadir)

5 Airborne Experiments

The PolarCube payload, MiniRad was part of NASA's IceBridge mission as a 'piggyback' airborne instrument (Figure 2a) aboard the NASA DC-8 (Oct 24 - Nov 02, 2016). At an aircraft altitude of ∼33,000 ft, images with resolution 380 m or better were captured. Calibrated sky scans obtained using measurements from a rooftop test at Boulder before the IceBridge mission with LN_2 and ambient targets for calibration are shown in Figure 7. The limb brightening effect for scan angles away from nadir, anticipated spectral behavior of the opaque and transparent channels, and scattering from the strut (near the right side of the curves) can be discerned from the plots. The higher level of noise in channels 2 and 3 (between 700 MHz and 1200 MHz) are possibly due to electromagnetic interference and are being debugged presently. First light images obtained from the 118 GHz spectrometer during these airborne experiments depict sharp land and water boundaries and indicate a well focused scanning reflector antenna system with high main beam efficiency (Figures 8a and 8b). Antenna temperature signatures obtained from 6 of 8 channels suggest the ability of the compact lumped element filterbank to separate chan-

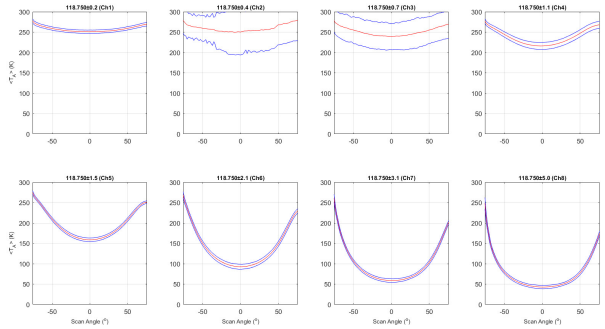

Figure 7. In these calibrated sky scans for each channel, the red curve is the mean antenna temperature averaged over 2100 scans (∼45 minutes). The RMS error per 5 ms sample is illustrated by the blue upper and lower curves. (Channels 2 and 3 show performance degradation possibly due to EMI.)

nels around the 118.75 GHz oxygen resonance. To further study the antenna system, along track nadir scans were extracted from images showing a sharp swing in brightness temperature such as at a land ocean boundary. The rate of change in antenna temperature as a function of the along track distance for these scans were found to be very similar to curves calculated using a spatial convolution of the computed far field antenna pattern and a 2D step function (Figures 9a, 9b). Note that the along track scan in Figure 9a is extracted from the image seen in Figure 8a and shows a dip close to the boundary because there is a drop in the antenna temperature for a 3 km wide region just before the coast line.

6 Conclusion

Images obtained from recent airborne tests with MiniRad indicate a stable, well-functioning radiometer with satisfactory prelaunch performance. They demonstrate it's ability to discern surface features with good accuracy indicating a focused antenna system as well as feasibility of using low cost 3D printed corrugated feed horns for millimeter wave radiometry. The compact, light-weight and low-cost 8 channel lumped element/microstrip filterbank also provides necessary distinction between channels with close-to desired bandwidths.

References

[1] A.J. Gasiewski and J.T. Johnson, "Statistical Temperature Profile Retrievals in Clear-Air Using Passive 118-GHz O_2 Observations," IEEE Trans. Geo. Sci. Rem. Sensing, vol. 31, 1993.

[2] Clarricoats, P.J.B. and Olver, A.D., 1984. "Corrugated horns for microwave antennas" (No. 18). let.

[3] L. Periasamy and A.J. Gasiewski, "Prelaunch Antenna Calibration of CubeSat MMW/SMMW Radiometers with Application to the PolarCube 3U Temperature Sounding Radiometer Mission." In IGARSS, 2016 IEEE International (pp. 5565-5568), (2016, July).

[4] J.A. Gordon, et al. "Millimeter-Wave Near-Field Measurements Using Coordinated Robotics." IEEE Transactions on Antennas and Propagation 63.12 (2015): 5351-5362.

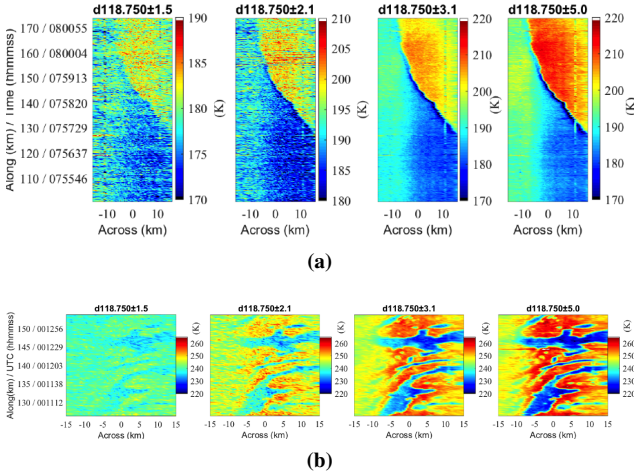

Figure 8. Antenna temperature maps (with scan bias removed) imaged by the instrument's most transparent channels: (a) land ocean boundary (b) Tierra del Fuego. (Aircraft Rexolite® window effect is present in images).

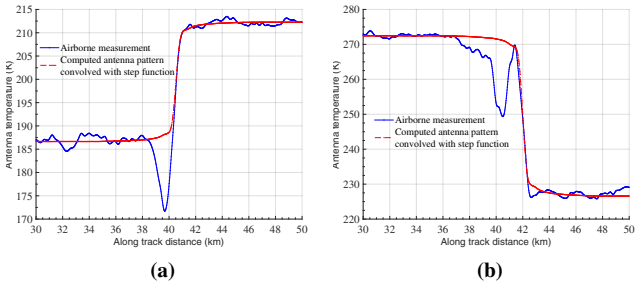

Figure 9. Comparisons between along track scans obtained from measurements (in blue) and theoretical estimates (in red)